Eur. Phys. J. D **12**, 171–179 (2000)

THE EUROPEAN PHYSICAL JOURNAL D

EDP Sciences

Structural characterisation of Ni clusters in AlN via X-ray absorption, X-ray diffraction and transmission electron microscopy

D. Zanghi[1], A. Traverse[1,a], J.-P. Dallas[2], and E. Snoeck[3]

[1] Laboratoire pour l'Utilisation du Rayonnement Électromagnétique (LURE), Bât. 209A, B.P. 34, 91898 Orsay Cedex, France
[2] Laboratoire de Chimie Métallurgie (LCM), 15 rue G. Urbain, 94407 Vitry Cedex, France
[3] Centre d'Élaboration de Matériaux et d'Études Structurales (CEMES), B.P. 4347, 31055 Toulouse Cedex 04, France

Received 25 August 1999 and Received in final form 8 February 2000

Abstract. Ni ions were implanted in bulk AlN with the goal to form embedded metallic clusters. Combining several characterisation techniques such as X-ray absorption spectroscopy, X-ray diffraction and high resolution transmission electron microscopy, we determined the lattice parameter of the Ni clusters that display a fcc crystalline structure. The average size increases when the ion fluence is increased or after a thermal treatment. Thanks to moiré fringes observed by high resolution transmission electron microscopy and to satellite peaks seen on the diffraction patterns, we concluded that the annealed Ni clusters orientate their (002) planes on the (101) of AlN. Moreover, the satellite positions allowed us to calculate Ni cluster average diameters, that are in agreement with average sizes deduced by X-ray absorption spectroscopy.

PACS. 61.46.+w Clusters, nanoparticles, and nanocrystalline materials – 61.10.Ht X-ray absorption spectroscopy: EXAFS, NEXAFS, XANES, etc. – 61.10.-i X-ray diffraction and scattering

1 Introduction

Small clusters have interesting and new physical properties that vary with the particle size. For example, small Co clusters in a polymer matrix [1] have an enhanced magnetic moment as compared to the bulk, whereas, for Co clusters made of 300 atoms embedded in a Cu matrix [2], a magnetic moment smaller than the bulk one has been measured. Gold clusters in alumina gel films [3] exhibit a strong red-shift whereas films of Au_N clusters [4] embedded in a porous alumina matrix show an opposite behaviour. Since the physical properties of these clusters strongly depend on their structure and shape, the atomic composition of the clusters and a precise structural characterisation, *i.e.* crystallographic structure, lattice parameters, together with average diameters and size dispersion are required to understand these different trends. Moreover, when the clusters are embedded in a matrix, an eventual interaction with the host atoms has to be detected and characterised.

Through *ab initio* calculations, the ability of X-ray techniques in building a structural model for such small particles was discussed in reference [5]. The authors considered X-ray absorption spectroscopy (XAS), useful to analyse the local environment around a given type of atom, atom of the clusters or atoms of the matrix, and X-ray diffraction (XRD) to get the crystalline structure and lattice parameter. They concluded on the necessity to combine several techniques to obtain all the above mentioned information. Both techniques, XAS and XRD, are in principle able to provide an average cluster size. The amplitude of the oscillations after the absorption coefficient edge is related to the average number of neighbors, hence to the cluster diameter, and the width of the diffraction peak is related to the size of the diffracting volume *via* the Sherrer's law. XAS and XRD are unable to give the cluster size dispersion, an information that can only be, in principle, obtained *via* transmission electron microscopy. Hence we chose to carry out these three techniques to characterise Ni clusters embedded in an AlN matrix.

In the last years, the ability of ion implantation to prepare small Cu clusters in the AlN matrix has been demonstrated [6, 7]. Preliminary results on Ni clusters prepared with the same technique, were given in reference [8], where X-ray absorption spectroscopy (XAS) was carried out to detect the cluster formation.

The goal of this article is to add new information on Ni clusters embedded in AlN. Data from X-ray diffraction (XRD) and high resolution transmission electron microscopy (HRTEM observations) are presented leading to a more precise description of their lattice parameter values, their average diameters and the way they are spatially distributed in the host lattice.

[a] e-mail: traverse@lure.u-psud.fr

Table 1. List of the samples with the implantation energies, the amounts of Ni in the target after implantation ($\pm$ 0.05 $\times$ 10^{17} Ni/cm^2) and Ni concentrations averaged over the FWHM of the profile.

incident energies (keV) and fluences 10^{17} Ni/cm^2		total implanted fluence 10^{17} Ni/cm^2	measured fluence as-impl. 10^{17} Ni/cm^2	Ni concentration
100	0.7	0.7	0.8	12%
100	0.77	0.86	1.11	16%
30	0.09			
100	1.5	1.5	1.56	18%
100	1.43	1.6	1.87	29%
30	0.17			
100	1.79	2.0	2.09	37%
30	0.21			
100	2.50	2.8	2.23	38%
30	0.30			

We found that the Ni clusters display a fcc crystallographic structure like bulk Ni with nearly the same lattice parameter. Average diameters of the order of 0.5 nm to 3 nm can be obtained. Because the clusters are close to each other, HRTEM did not permit us to separate the Ni particles, so no size dispersion data were obtained. Yet we show that, after annealing, the Ni clusters orientate themselves coherently on the AlN atomic planes. Thanks to the satellite peaks appearing in the diffraction induced by the coherency, we were able to extract diameters in agreement with those provided by XAS. We also explain the discrepancy between average diameters given by XAS and Sherrer's law. We also discussed the sensitivity of each technique, XAS, XRD and HRTEM in the particular case of size dispersed clusters.

2 Experimental details and results

2.1 Sample preparation

Polycrystalline bulk AlN has been implanted with the Irma implanter [9] at 300 K with Ni ions either at one (100 keV) or at two different incident energies (100 keV and 30 keV). Clusters prepared by ion implantation are expected to display some size dispersion because the implanted ion profile has a Gaussian shape. Thus particles that are formed in the middle of the profile might be larger than those formed in the tails. To compensate such an effect, ion implantation at several incident energies can be performed.

Various fluences allowed us to reach various Ni concentrations over more or less homogeneous profiles from the sample surface. In Table 1, samples with the implantation conditions are listed. In some cases, a post annealing treatment was done at 800 °C for 1 hour in a vacuum of the order of 10^{-4} Pa.

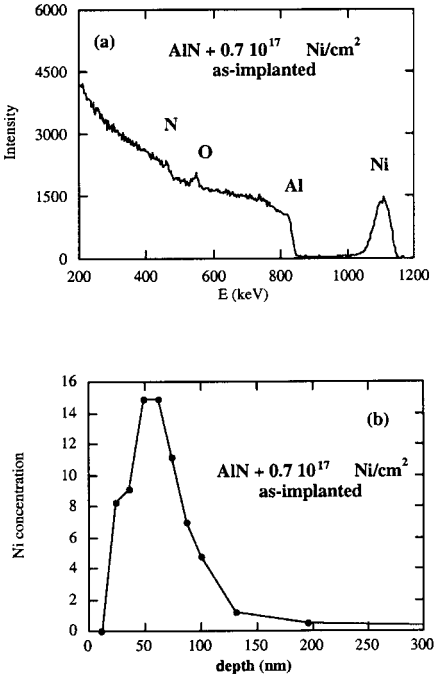

Fig. 1. (a) RBS spectrum and (b) Ni profile for a sample with 0.7×10^{17} Ni/cm^2 in the as-implanted state.

2.2 Characterisation

2.2.1 Rutherford backscattering spectrometry

RBS was performed on the Aramis accelerator [10] with 1.5 MeV He^+ particles that impinged perpendicularly to the target surface and were detected at 15° from the incident direction. The goal was to determine the number of Ni atoms actually in the target together with the in-depth distribution. The incident He energy was chosen in order to separate the Ni peak from the AlN signal. The number of Ni atoms present in the target was calculated, with an uncertainty of $\pm$ 0.05 $\times$ 10^{17} Ni/cm^2, by comparing the Ni peak area to the one of a standard sample made of Bi ions implanted in Si, measured in similar conditions. Values for as-implanted targets are given Table 1. As already described [6, 7], up to 2×10^{17} Ni/cm^2, the number of implanted ions in AlN is slightly enhanced as compared to the implanted fluence, an effect attributed to the insulating character of the matrix which perturbs the measurement of the ion current during implantation. For larger fluences, there is an effect of saturation.

Depth distributions were obtained by fitting of the whole spectrum using the RUMP code [11]. In Figure 1a is plotted a typical RBS spectrum for 0.7×10^{17} Ni/cm^2 as-implanted while in Figure 1b is reported the Ni profile deduced from the RBS measurement. Ni profiles are located at about 50 nm from the target surface and display a full width at half maximum (FWHM) of 60 nm. Ni concentrations averaged over the FWHM of the profile are given Table 1. Annealing induced a loss (about 10%) of Ni atoms that have diffused out of the target, leading to a Ni free surface layer.

In some cases, an Al_2O_3 surface layer, about 5 to 10 nm thick, has to be introduced in the fitting procedure to reproduce well the experimental RBS signal.

2.2.2 X-ray absorption spectroscopy

XAS was performed at LURE on the DCI ring running at 1.85 GeV and 300 mA. The scans were done at the K edge of Ni (the zero energy, 8333 eV, being fixed at the first inflection point) in an energy range of 1000 eV after the edge with 2 eV steps on a Ni foil and on the samples as implanted and also after annealing. Measurements on the Ni standard and on the samples (except two as-implanted samples with the lowest fluences) were performed at 80 K [12] using a cryostat allowing conversion electron yield (CEY) measurements, adapted to the samples studied here. We estimated the depth probed by the XAS experiments, "e", taking into account the study in reference [13] where "e" has been investigated for various photon incident energies. We found $e = 120$ nm, *i.e.* of the order of the implanted depth as measured by RBS. The absorption curves were treated in the usual way [14], extraction of the EXAFS oscillations, then calculation of the Fourier transform (FT). The FT of the Ni foil and of the sample implanted with 0.7×10^{17} Ni/cm^2 and 2.8×10^{17} Ni/cm^2 after annealing are compared Figure 2a. The similarity between the Fourier transforms for the samples and for the Ni foil is a strong indication of the cluster formation as we mentioned in reference [8].

The first peak of the FT was selected and back Fourier transformed. Assuming that neighbours of the Ni absorber are Ni atoms, hence that Ni clusters have formed, the obtained oscillation was fitted with the phase and amplitude extracted in the same conditions from the absorption curve for the Ni foil, in the frame of a single scattering process and the plane wave approximation [14]. Note that the studied samples are similar to the standard one, the Ni foil, with the same absorber-backscatterer pair. In such a favourable case, the uncertainty on the number of first neighbours was estimated to be $\pm$ 0.5. Figure 2b shows a comparison of the experimental and fitted modulus and imaginary parts of the Fourier transform of the first peak for the sample as-implanted with 1.5×10^{17} Ni/cm^2. Number of neighbours, Debye-Waller factors and distances are reported Table 2. The quality of the fit, indicated by a chi^2 factor around 3×10^{-3} in each case, supports our assumption of Ni clustering. We found that the number of neighbours is always smaller than 12 and that it increases with the implanted fluence and for the same sample, with the annealing treatment. The Debye-Waller factor does not change significantly after annealing, hence the thermal treatment induces mainly cluster diffusion leading to cluster growth.

In the case of small clusters, the average number of first neighbours around the absorber, N, is decreased as compared to the bulk, equal to 12 in the fcc structure, due to the fact that atoms located at the cluster surface have less neighbours than those located in the cluster core. If the cluster volume is divided in two parts, V_{core}, where

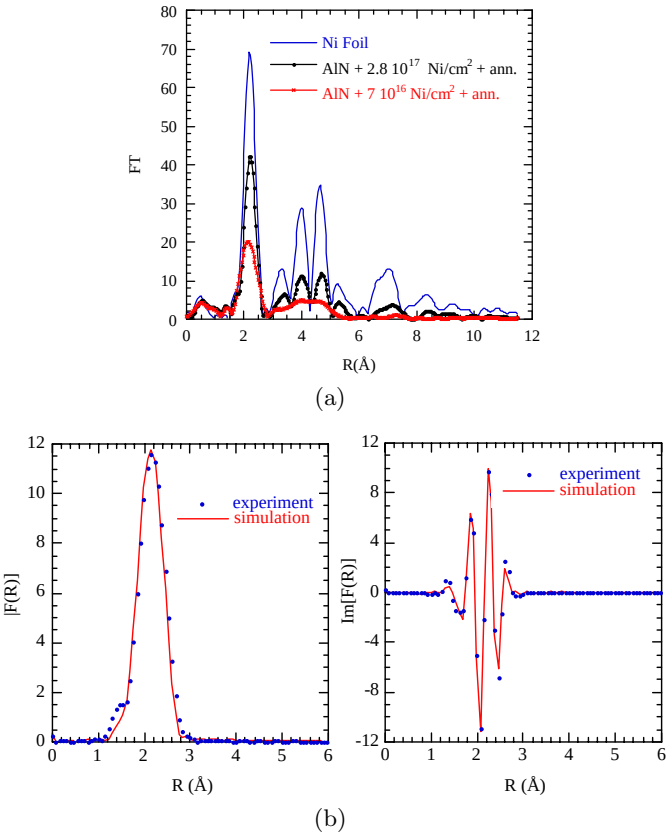

Fig. 2. (a) Fourier transforms for a Ni foil and for two Ni implanted AlN samples after annealing; (b) experimental and fitted modulus and imaginary parts of the Fourier transform of the first peak for the sample as-implanted with 1.5×10^{17} Ni/cm^2.

the number of first neighbors is 12 in a fcc structure, and V_{surface} where the number of first neighbors is $N_2 < 12$, we get an average number of neighbors

$$N = \frac{12V_{\text{core}} + N_2 V_{\text{surface}}}{V_{\text{core}} + V_{\text{surface}}}.$$

In a more general way, the relationship between the average number of neighbours measured on the first shell around the absorber, N, compared to the number of neighbours on the same shell, but in the bulk material, equal to 12, the distance to shell, R, and the average cluster diameter, D, is given in reference [15]

$$\frac{N}{12} = 1 - \frac{3}{2}\frac{R}{D}.$$

From data in Table 2 an average diameter for the Ni clusters is calculated, reported Table 3. As for other implantations in AlN [6,7], we find that D increases with the fluence and with the annealing treatment. The uncertainty on D, reported Table 3, was estimated from this formula and taking into account the uncertainty on N, $\pm$ 0.5.

As Ni clusters are embedded in the AlN matrix, one can ask why the oscillation fit does not require a matrix

Table 2. Number of Ni neighbors, distances and Debye-Waller factors, σ, as given by XAS for samples after ion implantation and after annealing.

sample	N	σ (nm)	R (nm)	N	σ (nm)	R (nm)
Ni foil	12		0.250			
	as implanted			annealed		
0.7×10^{17} Ni/cm^2				7	0.005	0.249
0.86×10^{17} Ni/cm^2				9.7	0.004	0.249
1.5×10^{17} Ni/cm^2	5.8	0.005	0.248	10		0.250
1.6×10^{17} Ni/cm^2	7	0.004	0.250	10	0.004	0.251
2.0×10^{17} Ni/cm^2	8.7	0.004	0.250	10.3		0.252
2.8×10^{17} Ni/cm^2	9	0.004	0.250	10.6	0.004	0.252

Table 3. Comparison of the lattice parameters and the average diameters for the Ni clusters obtained from XAS and XRD. Ratio of the peak intensities between the Ni (002) and (111) reflections.

Sample	XAS		XRD				XRD satellites
	a (nm) ± 0.003	D (nm)	a (nm) ± 0.0002	$\frac{I(002)}{I(111)}$	D (nm)	$\frac{n_a}{n_b}$	D (nm) ± 0.03
Ni ASTM file	0.3524						
1.5×10^{17} Ni/cm^2 as-impl.	0.349	0.7 $\pm$ 0.07					not measured
0.7×10^{17} Ni/cm^2 ann.	0.352	0.9 $\pm$ 0.1	0.3526	0.14	7.3 $\pm$ 0.8		no satellite
0.86×10^{17} Ni/cm^2 ann.	0.352	1.9 $\pm$ 0.5	0.3529	0.08	9.5 $\pm$ 1.0	13 11	2.3
1.5×10^{17} Ni/cm^2 ann.	0.354	2.2 $\pm$ 0.6	0.3533	0.14	7.6 $\pm$ 0.8	14 11	2.4
1.6×10^{17} Ni/cm^2 ann.	0.355	2.2 $\pm$ 0.6					not measured
2.0×10^{17} Ni/cm^2 as-impl.	0.354	1.4 $\pm$ 0.3	0.3550	0	7.2 $\pm$ 0.8		no satellite
2.8×10^{17} Ni/cm^2 as-impl.	0.354	1.5 $\pm$ 0.3	0.3565	0.10	9.0 $\pm$ 1.0		no satellite
2.8×10^{17} Ni/cm^2 ann.	0.356	3.2 $\pm$ 1.4	0.3568	0.21	22.3 $\pm$ 1.5	17 16	3.0

contribution such as Al or (and) N neighbours. The estimation of the proportion of Al and N atoms located at the cluster surface as compared to the number of atoms in the cluster volume depends on the cluster shape [16] that is not known precisely. However it cannot be larger than 1. Using the McKale tables [17], it is possible to calculate the amplitude for a Ni–Al absorber-backscatterer pair, f_{Al}, and for a Ni–Ni absorber-backscatterer one, f_{Ni}. On the k range from 50 nm^{-1} to 120 nm^{-1}, the ratio $f_{\mathrm{Al}}/f_{\mathrm{Ni}}$ is about 0.15 and even smaller for a Ni–N absorber-backscatterer pair. Hence for the smallest cluster with a diameter of 0.7 nm the contribution of the Al or N neighbours is at most 0.15 and becomes scarcely detectable for larger clusters.

From the Ni–Ni distances we calculated the lattice parameter, "a", for the Ni clusters, reported Table 3 in comparison with the lattice parameter given by the ASTM file No. 4-850. Taken into account the experimental uncertainty on R ($\pm$ 0.002 nm), hence on a ($\pm$ 0.003 nm), the agreement is good for the two lowest fluences. A small increase of a is observed for the two highest fluences that stays within the experimental accuracy.

2.2.3 HRTEM analyses

Bulk AlN samples implanted with 1.6 $\times 10^{17}$ Ni/cm^2 and then annealed, were prepared for TEM analyses in cross-section in order to study the size distribution. Samples were mechanically polished then ion milled (Ar, 5 keV) at liquid nitrogen temperature down to the electron transparency. TEM experiments were performed at CEMES on a Philips CM30 working at 300 kV whose point resolution

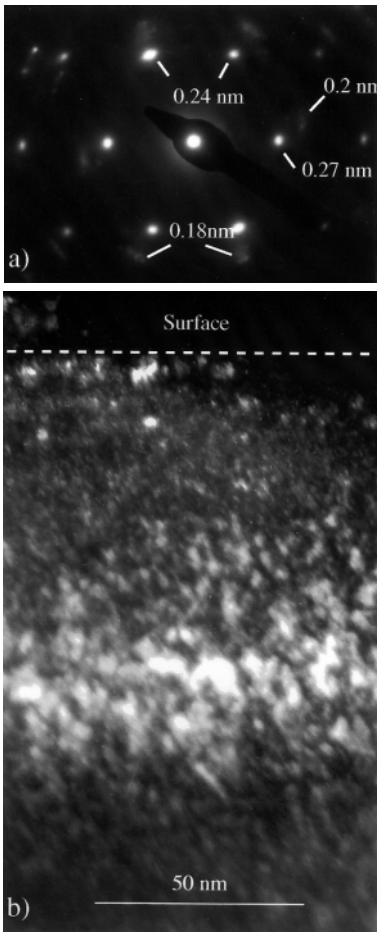

Fig. 3. (a) SAED pattern obtained on the 1.6×10^{17} Ni/cm^2 implanted and annealed sample and (b) 111-Ni dark field image

is 0.19 nm. Figure 3a is a selected area electron diffraction (SAED) pattern performed on a region close to the surface of the annealed sample. On this pattern the main spots can easily be indexed as 100 and 011 reflections of the AlN structure ($d_{100} = 0.269$ nm and $d_{011} = 0.237$ nm) indicating that the AlN matrix is observed along its [0-11] zone axis. The other more diffuse reflections are the 111 and 002 Bragg spots of Ni-fcc grains ($d_{111} = 0.203$ nm and $d_{002} = 0.176$ nm). The fact that the SAED of the Ni grains gives a dot pattern and not a ring one suggests that these grains display a particular orientation relative to the AlN matrix. Figure 3b is a dark field cross-section image realised selecting a 111-Ni reflection. All the bright contrasts therefore result from the Ni grains whose (111) planes diffracted on the selected spot. One can see that the main Ni contrast is located at about 60 nm far from the surface, in agreement with RBS data, but no individual grain can clearly be separated. This is due to the large amount of Ni clusters embedded in the matrix which makes them superimposed through the thickness of the TEM sample which is less than 10 nm in the thinnest part of the sample (close to the surface) and about 200 nm in the thicker regions. We thus have not been able to distinguish and separate the particles on such micrographs and no size distribution

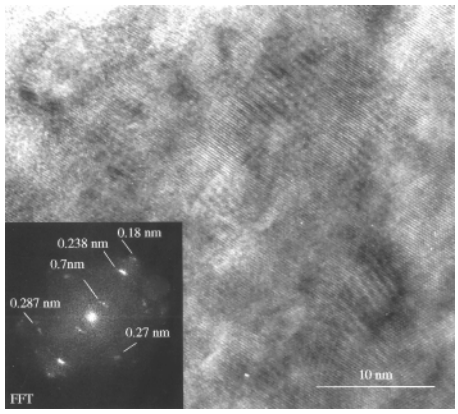

Fig. 4. HRTEM micrograph of Ni grains in AlN with its Fourier transform inset.

could be obtained. However, HRTEM experiments were carried out on areas located on the thinnest part of the sample, close to the implanted zone. Figure 4 shows such an HRETM micrograph with its Fourier transform (FFT) inset. Lattice and moiré fringes are observed on the image and the FFT permits us to measure their spacing. The $(100)_{\mathrm{AlN}}$, $(011)_{\mathrm{AlN}}$ and $(002)_{\mathrm{Ni}}$ planes are identified. The moiré spacing is about 0.7 nm and clearly comes from the interference between the $(002)_{\mathrm{Ni}}$ planes and the $(101)_{\mathrm{AlN}}$ ones (the theoretical value being 0.69 nm). The presence of such Ni-AlN moiré fringes confirms the particular orientation between the Ni grains and the matrix observed in SAED. It indicates that the particles display their $(002)_{\mathrm{Ni}}$ planes parallel to the $(101)_{\mathrm{AlN}}$ ones. The coherence size of the moirés gives an indication on the size of individual Ni grains which is about 10 nm on the studied area.

2.2.4 X-ray diffraction

XRD was performed at Laboratoire de Chimie Métallurgie using the Co k_α wavelength (0.179 nm). In order to get useful structural information, the probed depth has to be adjusted to the implanted one, measured by RBS. We chose to work in the asymmetric $\alpha - 2\Theta$ mode with α fixed and varying 2Θ. All samples were observed at $\alpha = 0.25°$ and 0.5°. Taking into account the optical index of AlN, we calculated that for $\alpha = 0.25°$, 0.5°, the typical analysed depths are 5 nm and 320 nm respectively. In order to observe most of the AlN peaks, 2Θ was varied from 30° to 100°.

A typical XRD pattern taken on an AlN sample before implantation is presented Figure 5a. Ten reflections corresponding to the wurtzite AlN structure are identified. Taking into account the (100), (002) and (110) reflections, we calculated lattice parameters $a = 0.311$ nm and $c = 0.499$ nm, in agreement with those of the the ASTM foil No. 25-1133, *i.e.* $a = 0.31114$ nm and $c = 0.49792$ nm. Values of the peak height ratio, $I(002)/I(111)$ and $I(101)/I(111)$ are 0.58 and 0.75 respectively, also in agreement with expected values of 0.60 and 0.80. The peak

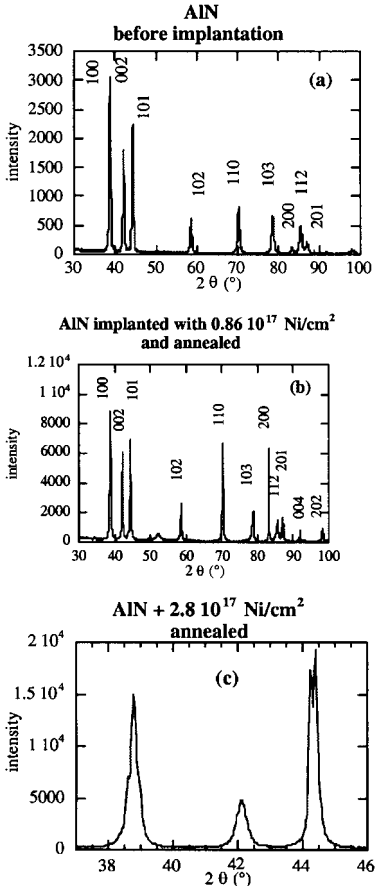

Fig. 5. (a) Diffraction pattern showing the AlN peaks corresponding to the wurtzite structure, before implantation, (b) diffraction pattern after implantation, (c) zoom on the (100), (101) and (102) AlN reflections in an implanted and annealed sample.

width can be interpreted as due to

(i) the instrumental broadening,
(ii) the size of the diffracting domains and
(iii) microdeformations of the crystalline lattice.

Assuming that the last effect is negligible in the non-implanted target, from the FWHM of the (100), (102) and (110) peaks obtained for an α value of 0.5°, and using the Sherrer's law, we extracted an average AlN grain diameter of 35 nm after subtraction of the instrumental broadening. We already mentioned [18] that the wurtzite structure is kept after implantation, *i.e.* that no amorphization is achieved under the amount of energy deposited by the implanted ions, as seen from Figure 5b. Yet, modifications of the relative peak intensities, for example (110) and (200), are observed together with splitting of some reflections that depends on the implanted fluence: an example is shown for the (100), (002) and (101) peaks (Fig. 5c).

Reflections belonging to Al_2O_3, *i.e.* (012), (104), (113) and (116), following the ASTM file No. 46-1212, are expected at $2\Theta = 29.84°$, 41.13°, 50.89° and 68.04°. Such

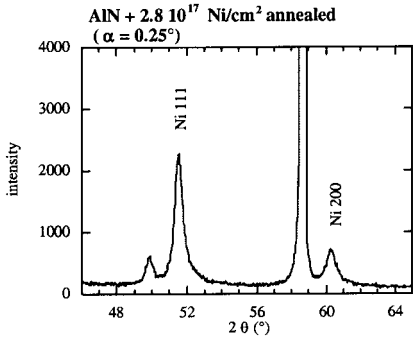

Fig. 6. The Ni (111) and (200) reflections.

reflections, with a very low intensity were detected for the lowest α value corresponding to the smallest probed depth, in the case of the 0.7×10^{17} Ni/cm^2 implanted sample after annealing in agreement with the fits of RBS spectra.

In Figure 6 is plotted the 2Θ range from 46° to 65° for the implanted samples. In addition to the (102) peak of AlN, two small peaks are observed which can be attributed to the (111) and (200) reflections of Ni in form of clusters with the fcc structure. Values of the Ni lattice parameter calculated from the (111) peak and from the (200) peak after subtraction of a background due to the AlN (102) reflection, reported in Table 3, are in agreement with those obtained from XAS.

The average diameter, D, of the Ni particles estimated from the FWHM of the (111) and (200) peaks are reported in Table 3, together with the peak height ratio $I(200)/I(111)$. Note that this last quantity is much smaller than the one expected for a fcc lattice, *i.e.* 0.40. Moreover, the particle diameters are in strong disagreement with values measured from XAS. As we ignored a possible contribution due to Ni lattice microdeformations, the whole peak width is attributed only to the cluster diameters and the instrumental broadening. However, introduction of another contribution should lead to larger diameters, *i.e.* should increase the observed discrepancy.

3 Interpretation and discussion

Two clear information arise from the data presented above. Ni implantation in AlN leads to cluster formation, as we had already demonstrated for Cu ions [6]. The interpretation is the same: the heat of formation of nickel nitride being positive [19], an Al site occupancy by Ni ions with N neighbours is forbidden, whereas a N site occupancy by Ni ions is not possible because of the negative character of this site. The only remaining possibility is thus to form precipitates. These clusters keep the fcc crystallographic structure of bulk Ni with the same lattice parameter value.

The AlN target is not amorphized. It is beyond the scope of this paper to precisely interpret the relative intensity modifications and the splitting that are observed

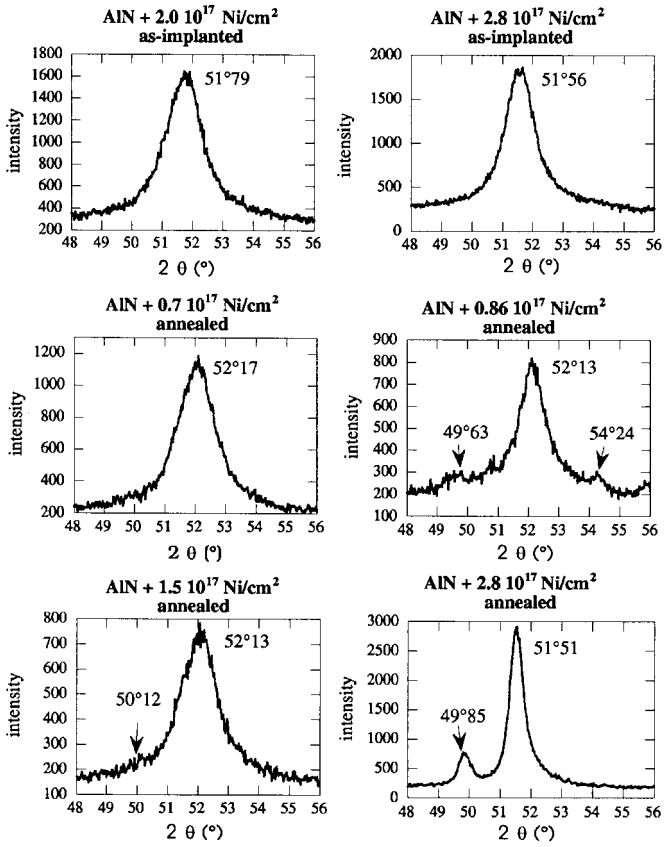

Fig. 7. Zoom on the (111) reflection of Ni for all the samples together with the angle values of the satellites used for the calculations.

on various reflections. We just suggest that the matrix probably suffers large deformations due to strain induced by the presence of the implanted ions, especially when they have formed clusters.

The discrepancy between average diameters of Ni clusters that are given by XAS, XRD and HRTEM is out of the experimental uncertainties. A first explanation comes from the sensitivity of each technique. If we believe the XAS size and take the example of the smallest clusters with $D = 0.7$ nm, the FWHM of the Ni (111) peak, using the Sherrer's law, should be of the order of 16°, it hence should disappear in the background. Small clusters below 1 nm are no more visible by TEM. In addition, the fact that they are superimposed in our samples may hide part of them, precluding any precise size determination, even less the size dispersion. The first step is thus to understand the presence of the observed (111) Ni reflections that are not expected for such small particles.

A careful observation of the (111) Ni reflections, shown Figure 7, reveals the existence of two small peaks located on both sides of the (111) reflection in the sample with 0.86×10^{17} Ni/cm^2 after annealing. One peak is located on the left of the (111) reflection for the two samples implanted with larger fluences and annealed. Such peaks are observed neither in the non-annealed samples nor in the less implanted one, although annealed. We first checked that these peaks do not belong to identified Ni_xAl_{1-x} compounds, such as Al_2Ni_3, Al_3Ni, Al_3Ni_2, Al_3Ni_5 and $AlNi_3$. These compounds could have form by interaction between the Ni atoms and the Al of the matrix.

Hence, we looked for another interpretation. HRTEM observations have shown the presence of moiré fringes due to interferences between $(002)_{Ni}$ planes and $(101)_{AlN}$ ones indicating that Ni clusters are preferentially orientate on the AlN planes.

Satellites, so-called Laue satellites, are currently observed in the XRD patterns of coherent multilayers [20,21] even recorded in the asymmetric mode. Such a system can be described as a stack of layers made of material a and b. Let n_a and n_b be the number of atomic planes with interplanar spacings d_a and d_b respectively. An average lattice spacing d_0 can be defined as

$$d_0 = \frac{n_a d_a + n_b d_b}{n_a + n_b} = \frac{\Lambda}{n} \tag{1}$$

where $n = n_a + n_b$ and

$$\Lambda = n_a d_a + n_b d_b \tag{2}$$

is the bilayer thickness or multilayer periodicity.

The diffracted intensity I of this system is

$$I = I_N(I_a + I_b + I_{ab}) \tag{3}$$

where the terms I_a and I_b represent the incoherent contributions in the XRD pattern of a and b whereas I_{ab} represents the contribution of one coherent a-b pair. I_N arises because the a-b pair is repeated N times. The mixed term I_{ab} gives rise to a peak located at d_0.

Such a picture of a coherent stack is clearly not appropriate to our system. It could be better to speak about Ni clusters embedded in larger AlN grains, that orientate their (002) planes under annealing on the (101) AlN ones. Let us assume that a is Ni and b is AlN, that $d_a = 0.1762$ nm corresponding to the Ni (002) interplanar spacing and $d_b = 0.2371$ nm corresponding to the AlN (101) interplanar spacing. If we also assume that n_a equals n_b, this leads to $d_0 = 0.2066$ nm, a distance close to the one corresponding to the Ni (111) reflection. This reflection appears to be due rather to the coherency between Ni and AlN planes, than to a reflection due to the Ni clusters only. The result is that

(i) a cluster diameter calculation from the peak FWHM appears meaningless,
(ii) the ratio $I(200)/I(111)$ is modified as compared to the expected one, as we observed experimentally (Tab. 3).

To go further and check the validity of the proposed picture, we have determined the actual values of n_a and n_b. First Λ and d_0 were extracted for each sample for α angles of 0.25° and 0.5°, from the two following equations where λ is the wavelength used to record the XRD patterns:

$$\lambda = 2\Lambda\Delta\sin\Theta, \tag{4}$$

$$\lambda = 2d_0\sin\Theta_0. \tag{5}$$

Then n_a and n_b were calculated from the Λ and d_0 values and solving equations (1, 2). $n_a d_a$ is considered as the average diameter, D, of the Ni clusters. Taking Θ and Θ_0 values as shown in Figure 7, n_a and n_b values together with calculated average diameters are reported Table 3, the latter being in agreement with the XAS values within the experimental uncertainties. Note that n_a and n_b values are close to each other, in agreement with the assumption made above to evaluate a first value of d_0. This point will be discussed later.

Although the satellite amplitudes are faint, except for the sample with the largest fluence, their angle positions allowed us, in a reliable way, to calculate cluster diameters that are in agreement with those estimated from XAS, making us confident in our interpretation. The smallness of the satellite intensities may be due to the fact that the plane orientation is not perfect and also because the a-b pair is not repeated several times, that makes the I_N term small in equation (3). Another step is to understand the clear evolution of the satellite amplitude when the fluence increases (Fig. 7). Gladyszewski [22] wrote a code that allows one to calculate the diffraction pattern, in the symmetric mode, of an assembly of textured grains made of several unit cells with parameters such as average grain size, D, deviation on the grain size, σ_D. The number of planes, n_a, n_b, in each type of unit cell for material a or b respectively, and their deviation, dv_a and dv_b, are also considered. Taking into account the polycrystalline character of the AlN matrix and neglecting the intensity peak modification that can occur in the asymmetric configuration, yet small on a short 2Θ range, we assumed that it is possible to use the code of Gladyszewski [22] even in the asymmetric configuration. Following the procedure used in reference [21], we compared experimental and calculated diffraction patterns corresponding to AlN and Ni unit cells inside grains of varying size keeping the values of d_a and d_b given above. The goal is not to fit the satellite intensities, but that tendencies come out. n_a, n_b as deduced from the satellite positions by the code are similar to the one given in Table 3. Moreover, with $dv_a = dv_b$, the two satellites are identical in amplitude as in the case of the 0.86×10^{17} Ni/cm^2 implanted and annealed sample whereas, with $dv_a = 0.3 dv_b$, the satellite at small angle is much higher than the other one (Fig. 8), as in the case of the two other samples. These latter cases correspond to a larger size distribution of the unit cells on AlN than on Ni. The bigger the clusters, the larger the size distribution on the AlN layers. Grain diameters of 2 nm and 6 nm were taken in the calculation respectively, reproducing rather well the experimental peak widths.

Two points remain to explain: the matching of the $Ni_{(002)}$ planes on the $AlN_{(101)}$ ones and the similarity between n_a and n_b values. The $AlN_{(101)}$ planes are made of Al atoms only, a favourable case, in line with the negative heat of formation of Al–Ni compounds as opposed to N–Ni ones. In the [0-11] direction the planes are separated by 0.587 nm and by 0.311 nm in the a direction, these two directions making an angle of 74°. Hence we suggest that Ni atoms occupy interstitial sites in such planes. The

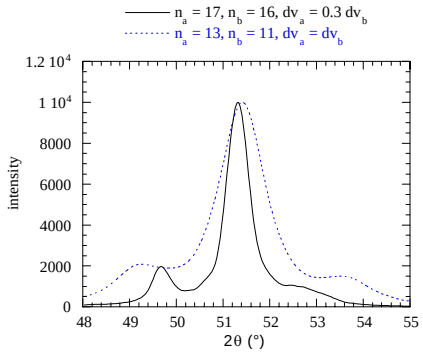

Fig. 8. Diffraction pattern calculated assuming textured grains of AlN and Ni with different numbers of Ni or AlN planes (n_a and n_b respectively) in the grains and similar ($dv_a = dv_b$) or different deviations in the grain size ($dv_a \neq dv_b$).

lattice mismatch is thus of 12% between the 0.311 nm in AlN and 0.352 in Ni.

As we said before, $n_a d_a$ is assimilated to D, the cluster diameter, hence $n_b d_b$ is the AlN thickness, that can also be considered as an average distance between the clusters. We made a crude evaluation of the average distance, $l_{\rm cl}$, between the Ni clusters, knowing the average volume of a cluster, $V_{\rm cl}$, the Ni atomic density, ρ, the implanted fluence, F, and the implantation profile width, $D_{\rm impl}$

$$l_{\rm cl}^3 = V_{\rm cl}\left(\frac{D_{\rm impl}\rho}{F} - 1\right).$$

Taking values such as 1.5×10^{17} Ni/cm^2 for F, 2 nm for the cluster diameter and 60 nm for $D_{\rm impl}$, we deduce $l_{\rm cl} \approx$ 1.1 D, *i.e.* $n_b d_b \approx 2.5 n_a d_a$. With $d_a = 0.1762$ nm and $d_b = 0.2371$ nm, this leads to $n_b/n_a \approx 0.8$ instead of about 1 as measured, which in view of such a crude picture is not too far. On the average, the clusters are separated by a distance of the same order of magnitude as their diameter, at least after annealing.

Satellites are not observed in the annealed but less concentrated sample. The average diameter of the clusters in this system as determined by XAS is 0.9 nm, which leads to satellites located at about 46.7° and 57.6°, *i.e.* in the tail of the (101) and (102) AlN reflections. The satellites are not observed in the as-implanted samples, although the cluster diameters, as determined by XAS, are in the good sensitivity range. It means that this is the annealing treatment which induces the rearrangement of the Ni clusters. We suggest that this process takes place *via* an interaction between the clusters in order to minimise the strain induced in the AlN lattice. This strain minimisation might be necessary especially in the situation where, due to the $D_{\rm impl}$ value, the clusters are close to each other. Implantations at much higher incident energy, leading to a larger $D_{\rm impl}$ value, might not induce such Ni cluster rearrangement. A similar effect of orientation was observed *via* HRTEM in the case of Cu implanted in AlN after annealing [23], and also, *via* channeling RBS, in the case of Pt implanted in single crystalline Al_2O_3 after annealing [24].

4 Conclusion

Ni cluster formation by ion implantation in AlN is in line with previous results on Cu [7]. Combining various techniques, XAS, XRD and HRTEM, we were able to characterise the fcc crystalline structure of the Ni clusters and to measure their lattice parameter.

These three techniques provided us average diameters in strong disagreement, by one order of magnitude. These discrepancies can be first explained by the different sensitivity of each technique, especially evidenced in the case of clusters that display a large size dispersion. XRD and HRTEM cannot detect small clusters located in the tails of the ion profile, whereas XAS "sees" all the clusters. Hence a direct comparison of results from these three techniques concerning Ni diameters is meaningless. The existence of such discrepancies in diameters coming from XAS and XRD when the size dispersion is large was not discussed in reference [5]; it appears particularly crucial through the experimental results presented here.

The moiré fringes observed in HRTEM indicated that under annealing the Ni precipitates orientate themselves with their (002) planes on the (111) AlN ones. This preferential orientation gave rise in the XRD pattern to satellites that allowed us to calculate the average size of the precipitates and the average distance between them. Then an agreement is found between diameters from XAS and XRD. This reveals that XAS is the adequate technique to get access to average cluster diameter, especially in the case of this size range, *i.e.* around 1 nm. To our knowledge, this is the first time that a comparison of cluster diameters from XAS and satellite angular positions is done.

A last conclusion is that the Ni clusters are surrounded by Al atoms, at least after annealing. The electronic distribution of the Ni atoms located at the cluster surface is certainly different due to the Al vicinity, from the one of Ni atoms in the cluster core. We suggest that an explanation of the opposite behaviour of the Co clusters embedded either in a polymer or in a Cu matrix in terms of the magnetic moment should be looked for in the different cluster environment.

We thank the staff around Irma and Aramis for help during the ion beam experiments. M. Masse from École de Chimie de Paris and C. Barbeau from Laboratoire de Métallurgie Physique de Poitiers are acknowledged for the annealing treatments. We are grateful to G. Gladyszewski for allowing us to use his code. P. Baules from CEMES and G. Gladyszewski made very sensible comments allowing us to greatly improve our article.

References

1. M. Respaud, J.M. Broto, H. Rakoto, A.R. Fert, L. Thomas, B. Barbara, M. Verelst, E. Snoeck, P. Lecante, A. Mosset, J. Osuna, T. Ould Ely, A. Amiens, B. Chaudret, Phys. Rev. B **57**, 2925 (1998).
2. D.A. Eastham, Y. Qiang, T.H. Maddock, J. Kraft, J.-P. Schille, G.S. Thompson, H. Haberland, J. Phys. Cond. Matt. **9**, L497 (1997).
3. Y. Hosoya, T. Suga, T. Yanagawa, Y. Kurokawa, J. Appl. Phys. **81**, 1475 (1997).
4. B. Palpant, B. Prével, J. Lermé, E. Cottancin, M. Pellarin, M. Treilleux, A. Perez, J.L. Vialle, M. Broyer, Phys. Rev. B **57**, 1963 (1998).
5. D.C. Bazin, D.A.A. Sayers, J.J. Rehr, J. Phys. Chem. **101**, 11040 (1997).
6. M. Borowski, A. Traverse, J. Mimault, Acta Phys. Polon. A **86**, 713 (1994).
7. A. Traverse, P. Parent, J. Mimault, S. Hagège, J. Du, Nucl. Instrum. Meth. B **84**, 204 (1994).
8. A. Traverse, Hyperf. Interact. **110**, 159 (1997).
9. J. Chaumont, F. Lalu, M. Salomé, A.M. Lamoise, Nucl. Instrum. Meth. **189**, 193 (1981).
10. H. Bernas, J. Chaumont, E. Cottereau, R. Meunier, A. Traverse, C. Clerc, O. Kaitasov, F. Lalu, D. Le Du, G. Moroy, M. Salomé, Nucl. Instrum. Meth. B **62**, 416 (1992).
11. L.R. Doolittle, Nucl. Instrum. Meth. B **15**, 227 (1986).
12. J. Mimault, J.J. Faix, T. Girardeau, M. Jaouen, G. Tourillon, Meas. Sci. Technol. **5**, 482 (1994).
13. T. Girardeau, J. Mimault, M. Jaouen, P. Chartier, G. Tourillon, Phys. Rev. B **46**, 7144 (1992).
14. A. Michalowicz, *Logiciels pour la chimie* (Ed. Soc. Française de Chimie, Paris, 1991), p. 102.
15. M. Borowski, J. Phys. IV France **7**, C2-259 (1997).
16. R. van Hardeveld, F. Hartog, Surf. Sci. **15**, 189 (1969).
17. A.G. McKale, J. Am. Chem. Soc. **110**, 3763 (1988).
18. M. Borowski, A. Traverse, J.P. Dallas, J. Mater. Res. **10**, 3136 (1995).
19. *Smithells Metals Reference Book*, edited by E.A. Brandes, 6th edn. (Butterworth, London, 1983).
20. C. Michaelsen, Philos. Mag. A **72**, 813 (1995).
21. L. Bimbault, K.F. Badawi, Ph. Goudeau, J. Mimault, O. Proux, J. Phys. IV Colloq. France **6**, C7-43 (1996).
22. G. Gladyszewski, Thin Solid Fims **170**, 99 (1989).
23. J. Du, A. Traverse, S. Hagège, Electron Microscopy, *EUREM 92*, Vol. 2, Granada, Spain, 1992.
24. E. Alves, R.C. da Silva, O. Conde, M.F. da Silva, J.C. Soares, Nucl. Instrum. Meth. B **148**, 1049 (1999).